PRAMANA — journal of physics
© Indian Academy of Sciences
Vol. 84, No. 5
May 2015
pp. 717–730

Transport models for relativistic heavy-ion collisions at Relativistic Heavy Ion Collider and Large Hadron Collider

SUBRATA PAL
Department of Nuclear and Atomic Physics, Tata Institute of Fundamental Research, Homi Bhabha Road, Mumbai 400 005, India
E-mail: spal@tifr.res.in

DOI: 10.1007/s12043-015-0976-x; ***e*Publication:** 29 April 2015

Abstract. We review the transport models that are widely used to study the properties of the quark-gluon plasma formed in relativistic heavy-ion collisions at RHIC and LHC. We show that transport model analysis of two important and complementary observables, the anisotropic flow of bulk hadrons and suppression of hadron yields at high transverse momentum, provide exciting new information on the properties of the plasma formed.

Keywords. Quark-gluon plasma; transport models; flow; jet quenching.

PACS Nos 25.75.−q; 12.38.Mh; 21.10.Lx; 24.85.+p

1. Introduction

High-energy heavy-ion collisions at the Relativistic Heavy Ion Collider (RHIC) [1–4] and recently at the Large Hadron Collider (LHC) [5–7] have provided conclusive evidence of the formation of a quark-gluon plasma (QGP) that behaves like a near perfect fluid [8,9]. Evidence of this is provided by the relativistic viscous hydrodynamic model analysis of anisotropic/elliptic flow data that requires an extremely small shear viscosity to entropy density ratio of $\eta/s \leq 0.10$–0.20 depending on the initial conditions [10,11]. However, there is a growing body of evidence that indicates the breakdown of hydrodynamical behaviour especially in peripheral collisions, at intermediate/large transverse momentum $p_{\mathrm{T}} > 2$ GeV/c, and at large viscosities. This stems essentially when the single-particle distribution function deviates largely from its equilibrium value f_{eq} [10,12,13].

In contrast to hydrodynamics, transport approaches do not invoke gradient expansion in velocity (or viscosity), and thus can be reliably used to study nonequilibrium momentum distribution of particles at all p_{T} and at large viscosities. Further, as transport models treat chemical and thermal freeze-out dynamically, they serve as natural and powerful tools for studying freeze-out dynamics [14,15].

While the free-streaming of particles in the kinetic theory drive the system out of equilibrium, the (short-range) N-body collisions lead to a finite mean free path $\lambda = 1/(\rho\sigma)$ and help to build up collective flow as well as enforce isotropization and thermalization of the particle momentum. In the parton cascade approach, the equation of state (EoS) corresponds to a free gas with sound velocity $c_s^2 = \mathrm{d}P/\mathrm{d}\epsilon = 1/3$. The (long-range) mean-field interaction in the transport equation causes the EoS to deviate from the ideal gas value. On the other hand, in ideal hydrodynamics the mean free path is assumed vanishing and the magnitude of anisotropic flow depends strongly on the EoS [16]. In any case, while a finite value of λ is required in transport, an EoS that includes deconfined QGP phase with a small η/s is essential in viscous hydrodynamics for the generation of the observed large momentum anisotropy and its saturation at moderate p_T.

The parton transport models have been quite successful in explaining at the RHIC and LHC energies, the centrality and pseudorapidity dependence of p_T-averaged value of the elliptic and triangular flow $\langle v_n \rangle$ ($n = 2, 3$), the suppression of $v_2(p_T)$ at intermediate and large p_T [17,18], the scaling of $v_2(p_T)$ with initial spatial eccentricity ϵ_2 [19,20], the constituent quark-number scaling $v_n/n_q^{n/2}$ ($n = 2$–4) of hadrons at intermediate p_T [21], and recently the correlations among event planes for different flow harmonics [22] over a wide pseudorapidity range. All these explanations suggest that the matter formed is close to local thermal equilibrium and collective flow develops in the partonic stage.

The phenomenon of jet quenching, or the modification of hard jets in the dense matter is the other striking discovery at RHIC. The observed suppression of high-p_T hadrons [23,24] in central collisions relative to both peripheral and nucleon–nucleon collision has been well established as due to the parton energy loss via medium-induced gluon emission [25–31] and somewhat by elastic scattering. Microscopic transport calculations provide a realistic and direct way to understand the jet interaction with the evolving medium, and the medium's response in broadening the jet momentum and redistribution of the lost energy via parton scatterings [18,32,33].

In this article, we shall review the transport models that have been successfully employed at the RHIC and LHC energy regime. We shall focus on the two important observables, the anisotropic flow and jet quenching, that in conjunction with the transport model results have provided new and interesting insights into the properties of the QGP formed.

2. Transport models

The relevant microscopic degrees of freedom (partons, hadrons, strings) in the Boltzmann–Vlasov transport theory depend primarily on the energy of the colliding nuclei. For collisions at RHIC and LHC, a transport model may involve four main components depending on the observable of interest: (1) the initial conditions, (2) parton dynamics, (3) parton to hadron formation, and (4) hadronic interactions. In this section, we shall present four transport models that are widely used in the study of ultrarelativstic heavy-ion collisions at the RHIC and LHC regime, namely the AMPT [17], BAMPS [34], PHSD [35], and the Catania group [20,36,37]. Apart from their numerical implementation, the models vary fundamentally in the underlying calculation of the collision cross-sections, (non-)inclusion of mean field and hadronization procedure.

2.1 *Initial conditions*

The initial conditions describe the spatial and momentum distribution either for the participating nucleons or for partons. In a multiphase transport (AMPT) model [17], the radial density of the two colliding nuclei is taken to be Woods–Saxon distribution and is based on Glauber model. Particle production from nucleon–nucleon collisions is described by hard processes (jet and minijet partons) at $p_T > p_0$ and soft process (string excitations) at $p_T \leq p_0$ with an effective cross-section σ_{soft} as implemented in the HIJING model [38]. In HIJING 2.0 [39], the Duke–Owens parametrization [40] of the parton distribution functions has been updated with the modern Glück–Reya–Vogt (GRV) parametrization [41]. As the gluon distribution at small momentum fraction x is much larger in GRV, instead of a fixed value for $(p_0, \sigma_{\text{soft}})$ as in HIJING 1.0, an energy-dependent cut-off for $p_0(\sqrt{s})$ and $\sigma_{\text{soft}}(\sqrt{s})$ are used to fit experimental data on total and inelastic cross-sections in $p + p/\bar{p}$ collisions [39]. For the nuclear parton distribution function (PDF), HIJING employs the functional form $f_a^A(x, Q^2) = AR_a^A(x, Q^2) f_a^N(x, Q^2)$, where f_a^N is the PDF in a nucleon and $R_a^A(x, Q^2)$ is the nuclear modification factor of quarks and gluons ($a \equiv q, g$). An impact parameter dependence of shadowing is taken as $s_a(b) = (5s_a/3)(1 - b^2/R_a^2)$ where $R_A \sim A^{1/3}$ is the nuclear size. $s_q = 0.1$ is fixed from deep inelastic scattering data and s_g can be estimated from fits to the measured charged particle pseudorapidity density $\mathrm{d}N_{\text{ch}}/\mathrm{d}\eta$ in heavy-ion collisions.

In a Boltzmann approach to multiparticle scattering (BAMPS) model [34], the starting point is the semiclassical minijet gluons from hard nucleon–nucleon collisions; the initial gluon rapidity $\mathrm{d}N_{\text{g}}/\mathrm{d}y$ is fixed to reproduce the final charged hadron pseudorapidity density $\mathrm{d}N_{\text{ch}}/\mathrm{d}\eta$.

The parton-hadron-string-dynamics (PHSD) [35] model is a microscopic covariant transport model where the hadronic part is essentially the conventional HSD approach [42] and the partonic dynamics is based on the dynamical quasiparticle model (DPQM) [43,44] which describes QCD properties in terms of single-particle Green's functions. The initial phase-space distributions of the projectile and the target nuclei are determined in the local Thomas Fermi limit. Initial soft nucleon–nucleon interactions are described by the excitation of two colour-neutral strings which decay in time to the known hadrons (mesons, baryons, antibaryons); the initial hard processes are described by pQCD. In PHSD, the nuclear shadowing of the PDFs are as implemented in HIJING.

QCD calculations on a lattice indicate a cross-over to a colour deconfined and chirally symmetric restored phase at the critical temperature $T_{\text{c}} \simeq 170$ MeV and energy density $\epsilon_{\text{c}} \simeq 700\ \text{GeV/fm}^3$ [45,46]. As the central energy densities reached at RHIC and LHC are much higher than ϵ_{c}, the existence of strings is questionable. This leads to string melting version of AMPT and a natural formation of parton degrees of freedom in PHSD where the initial strings are melted to their constituent partons resulting in a substantial initial parton density of the medium.

2.2 *Parton transport*

The basic equation for the parton interactions and evolution is described by the equations of motion of the Wigner distribution function $f_a(\mathbf{x}, \mathbf{p}, t)$ in phase-space

$$p^\mu \partial_\mu f_a(\mathbf{x}, \mathbf{p}, t) + M(\mathbf{x}, t)\partial_\mu M(\mathbf{x}, t)\partial_p^\mu f_a(\mathbf{x}, \mathbf{p}, t) = \mathcal{C}(\mathbf{x}, \mathbf{p}, t), \tag{1}$$

where the first term corresponds to free streaming of partons and the second term represents the effects of the (scalar/vector/tensor) mean fields that provide the interaction. The collision term can be expressed as

$$
\begin{aligned}
\mathcal{C}(\mathbf{x}, \mathbf{p}, t) = & \sum_{m} \sum_{b_i} \int \prod_{i=1}^{m} \mathrm{d}p_{b_i} f_{b_i}(\mathbf{x}, \mathbf{p_{b_i}}, t) \sum_{n} \sum_{c_j} \int \prod_{j=1}^{n} \mathrm{d}p_{c_j} |M_{m\to n}|^2 \\
& \times (2\pi)^4 \delta^4 \left(\sum_{k=1}^{m} p_{b_k} - \sum_{l=1}^{n} p_{c_l} \right) \\
& \times \left[-\sum_{q=1}^{m} \delta_{ab_q} \delta^3(\mathbf{p} - \mathbf{p_{b_q}}) + \sum_{r=1}^{n} \delta_{ac_r} \delta^3(\mathbf{p} - \mathbf{p_{c_r}}) \right]. \qquad (2)
\end{aligned}
$$

Here $\mathrm{d}p_{b_i} \equiv \mathrm{d}^3 p_{b_i}/[(2\pi)^3 2E_{b_i}]$ and $M_{m\to n}$ denote the matrix element of the multi-parton interaction $m \to n$.

At the RHIC and LHC energies, the partonic scattering is expected to dominate over the mean-field effects. In the parton cascade in AMPT (that uses Zhang's parton cascade (ZPC) model [47]) and in BAMPS, the elastic scattering cross-section for $gg \leftrightarrow gg$ is calculated from pQCD as $\mathrm{d}\sigma_{\mathrm{gg}}/\mathrm{d}t \simeq 9\pi\alpha_{\mathrm{s}}^2/2(t - m_{\mathrm{D}}^2)^2$, where t is the usual Mandelstam variable and α_{s} is the strong coupling constant. While the Debye screening mass m_{D} can be calculated locally from the gluon distribution function [34] and thus temperature-dependent, in AMPT, m_{D} is varied to study the effects of parton cross-section σ in heavy-ion collision. Here, the effective EoS exhibits [48] a stiff QGP phase with a speed of sound $c_{\mathrm{s}}^2 = \mathrm{d}P/\mathrm{d}\varepsilon \approx 0.32$, and in the mixed phase c_{s}^2 gradually decreases to a minimum of about 0.1 that is consistent with the lattice QCD predictions [45,46].

BAMPS transport further incorporates inelastic $gg \leftrightarrow ggg$ pQCD bremsstrahlung process via an effective matrix element [34]

$$
\left|\mathcal{M}_{\mathrm{gg}\to\mathrm{ggg}}\right|^2 = \frac{72\pi^2\alpha_{\mathrm{s}}^2 s^2}{(\mathbf{q}_\perp^2 + m_{\mathrm{D}}^2)^2} \frac{48\pi\alpha_{\mathrm{s}}\mathbf{q}_\perp^2}{\mathbf{k}_\perp^2[(\mathbf{k}_\perp - \mathbf{q}_\perp)^2 + m_{\mathrm{D}}^2]} \Theta\left(\frac{\Lambda_{\mathrm{g}}}{\gamma} - \tau\right), \qquad (3)
$$

where $\mathbf{q}_\perp$ and $\mathbf{k}_\perp$ denote the perpendicular components of the momentum transfer and the radiated gluon momentum in the c.m. frame of the colliding partons, respectively. These inelastic processes were shown to speed up the equilibration times of the gluon plasma to within 1 fm/c and could also explain both the elliptic flow and jet quenching data at RHIC within the BAMPS framework. As we shall demonstrate, even in the absence of $gg \leftrightarrow ggg$ scatterings, the large initial parton density in the string melting AMPT can generate large collective flow as well as a largely opaque system to inject sufficient energy loss of the jets in the medium.

In the equilibrium limit of a massless plasma at high T, the shear viscosity becomes $\eta = (4/15)\langle p\rangle\rho\lambda$ and the entropy density $s = \rho(4 - \mu_{\mathrm{B}}/T)$ with $\langle p\rangle$ the average momentum, ρ the local parton density, $\lambda = 1/\rho\sigma$ the mean free path and μ_{B} the baryon chemical potential. The transport cross-section can then be expressed as $\sigma_{\mathrm{tr}} = (4/15)\langle p\rangle/[\rho(4 - \mu_{\mathrm{B}}/T)(\eta/s)]$. Alternatively, σ_{tr} can then be estimated for various (temperature-dependent or independent) choices of the η/s ratio of the plasma. This approach, adopted in the parton transport model studies by the Catania group [20,36,37], allows for a direct comparison with the results from the relativistic viscous hydrodynamic models.

In the AMPT model, the Boltzmann equations are solved within ZPC parton cascade [47], where partons undergo two-body scattering whenever they approach each other at a distance $r \leq \sqrt{\sigma_{\mathrm{gg}}/\pi}$. In this geometrical scattering scheme, the space is divided into small cells, and collisions between partons within the same and neighbouring cells are considered. These collisions are ordered (in time) depending on their interparticle separation. In contrast, the parton cascade in BAMPS and Catania group is based on stochastic interpretation of the transition rates for on-shell partons within each small cell in space and within a certain time interval. Further, to reduce statistical fluctuations in a cell, a test particle technique is adopted that amplifies the gluon density by N_{test} and the cross-section is accordingly reduced by the same factor to obtain the same mean free path. In all these models, the partons propagate along straight line trajectories in between their collisions.

The PHSD model [35] invokes off-shell parton transport equations in phase-space representation where the field quanta are described via dressed propagators with complex self-energies. The real part of the self-energies corresponds to mean-field (scalar, vector, tensor) potentials and the imaginary parts provide information about the lifetime and/or reaction rates of the 'quasiparticles'. Thus, it generates a strongly interacting system and allows for an elegant interpretation of the lattice QCD results for the thermodynamic quantities and correlators [49]. In contrast to massless gluons and valence quark masses in AMPT and BAMPS, space-time (and hence temperature) dependent masses have been used in the PHSD model and in the transport model of the Catania group. The dynamical quasiparticle masses are taken as $m_{\mathrm{g}}^2 \simeq [(N_{\mathrm{c}} + N_{\mathrm{f}}/2)T^2/g^2]^{-1}$ and $m_{\mathrm{q}}^2 \simeq (N_{\mathrm{c}}^2 - 1)g^2T^2/8N_{\mathrm{c}}$, where N_{c} and N_{f} are the number of colours and flavours, respectively and $g \equiv g(T)$ is the temperature-dependent running coupling constant.

2.3 *Hadronization*

One of the simplest procedures to achieve hadronization is by converting a gluon after its freeze-out to a pion with equal probability for the three charge states according to the parton–hadron duality, as used in BAMPS [34]. On the other hand, the minijet partons after freeze-out can be traced back to their parent nucleons to form excited strings. Hadronization can then be achieved by fragmentation of these strings by the Lund string model as has been employed in default AMPT. In the string melting version of AMPT [17], the minijet partons as well as hard partons undergo hadronization at freeze-out via a simple quark coalescence in phase-space by combining the nearest two-partons into a meson and three (anti)quarks into an (anti)baryon. As parton recombination leads to a continuous spectrum, it is impossible to conserve four-momentum. Thus, three-momentum is generally conserved and the energy conservation is violated which however is small ($\sim$2%) in an event. This problem is circumvented in the PHSD model [35] that invokes a dynamical description of parton to hadron production by employing local covariant transition rates for $q + \bar{q} \rightarrow M$ and $q_1 + q_2 + q_3 \rightarrow B$ within explicit energy, momentum as well as flavour current conservation to form colour neutral hadrons.

2.4 *Hadron transport*

The hadron transport models for heavy-ion collisions, such as ART [50], HSD [42], RQMD [51], UrQMD [52] either have hadrons as degrees of freedom or strings which fragment to hadrons. These models include all possible baryon–baryon, baryon–meson and meson–meson elastic and inelastic collisions whose cross-sections are fitted to scattering data or taken from phenomenological models. As it may include mean-field potentials (for baryons and kaons) the effects of hadronic EoS can be explored. Consequently, hadron transport models are well suited to study heavy-ion collisions in the energy range $\sqrt{s_{NN}} \leq 17$ GeV where hadronic effects dominate or act as an afterburner to hadron production from partons as employed in AMPT and PHSD models.

3. Results and discussions in the transport models

3.1 *Constraining the initial parameters*

The measured centrality dependence of hadron yield can be used to constrain the (gluon) shadowing, thereby allowing a proper distribution of initial (cold) partons in the colliding nuclei [39,53]. Figure 1 shows the charged particle pseudorapidity density per participant pair, as a function of centrality of collision characterized by the average number of participating nucleons $\langle N_{\mathrm{part}}\rangle$ in the AMPT model and data. The AMPT calculations at both the RHIC and LHC energies were performed at the same values of strong coupling constant $\alpha_{\mathrm{s}} = 0.33$ and screening mass $m_{\mathrm{D}} = 3.23$ fm^{-1} [57] that correspond to parton–parton elastic scattering cross-section of $\sigma \approx 9\pi\alpha_{\mathrm{s}}^2/(2m_{\mathrm{D}}^2) \approx 1.5$ mb. The initial condition for the gluon shadowing parameter was set at $s_{\mathrm{g}} = 0.10$–0.17 at RHIC and $s_{\mathrm{g}} = 0.16$–0.17 at LHC that agrees well with the data within the experimental uncertainty. Due to abundant (mini)jet production in Pb+Pb collisions at LHC, the ALICE multiplicity results [56] are quite sensitive to nuclear distortions at small x and provide a much stringent constraint on the gluon shadowing of $s_{\mathrm{g}} \simeq 0.17$. The estimated values of s_{g} in AMPT are consistently smaller than the HIJING 2.0 [39] estimate without final-state scatterings. This suggests the importance of parton dynamics, that lead to considerable energy redistribution resulting in the reduction of charged particle yield by $\sim$15% at both RHIC and LHC.

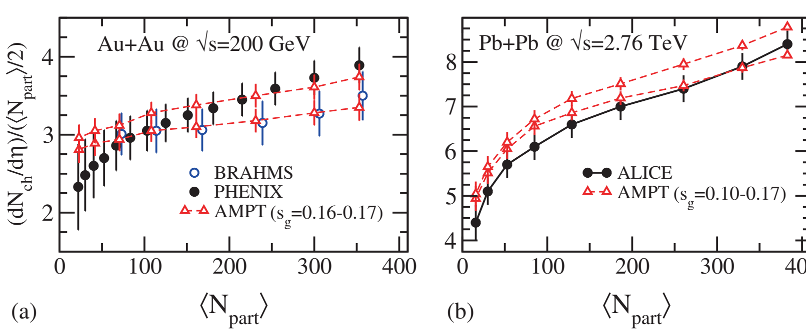

Figure 1. $\mathrm{d}N_{\mathrm{ch}}/\mathrm{d}\eta$ at midrapidity per participant nucleon pair as a function of $\langle N_{\mathrm{part}}\rangle$. The results are from AMPT calculations (triangles) with gluon shadowing $s_{\mathrm{g}} = 0.10$–0.17 at RHIC (**a**) and with $s_{\mathrm{g}} = 0.16$–0.17 at LHC (**b**) as compared with the data (circles) from BRAHMS [54] and PHENIX [55] at RHIC and ALICE [56] at LHC.

3.2 *Anisotropic flow*

Partonic interactions within the initial spatially asymmetric collision zone drives uneven pressure gradients that manifest in anisotropic emission of particles leading to collective flow [58,59]. The magnitude of this flow is characterized [19,60] by the Fourier coefficients $v_n = \langle \cos(n[\phi - \Psi_n]) \rangle$ as elliptic (v_2), triangular (v_3) flow estimated with respect to their participant event planes Ψ_n. Flow can also be determined using the two-particle cumulant method $v_n\{2\} = \sqrt{\langle \cos(n\Delta\phi) \rangle}$, where $\Delta\phi$ is the azimuthal angle difference between particle pairs within the same event. Compared to the former event-plane method, the 2-particle cumulant method effectively gives larger v_n due to nonflow effects especially at large $p_{\rm T}$.

The importance of partonic degrees of freedom in generating the large anisotropic flow v_2 was realized about a decade earlier, when purely hadronic transport models such as UrQMD [61] and HSD [62] models severely underpredicted the measured v_2. Evidence of the formation of a strongly coupled partonic medium at RHIC was demonstrated in the Molnar's parton cascade (MPC) model [63] that required [64] partonic cross-section $\sigma_{\rm gg} \sim 30$ mb, much larger than the pQCD estimate of 3 mb, to mimic v_2 from ideal hydrodynamics and data.

Figure 2 (top panel) compares the predictions of the string melting version of AMPT with the RHIC data [65,66] for the $p_{\rm T}$ dependence of v_2 and v_3 for charged hadrons at various centralities. In this comparison, the same procedure (event-plane or cumulant) has been used in both the theoretical calculations and data. The large initial parton density due to melted strings in AMPT and/or repulsive mean field in the PHSD [35] are found essential to reproduce the data.

In figure 2 (bottom panels), the AMPT results for the centrality dependence of $v_n\{2\}$ ($n = 2$–6) in Pb+Pb collisions at LHC is found to agree quite well with the data [67,68]. The magnitude of anisotropic flow at LHC and RHIC are seen to be similar. The enhanced parton density at the LHC energy that is expected to produce larger v_2 appears to be compensated by faster expansion of the evolving medium due to larger flow.

With increasing impact parameter b, larger initial eccentricity $\epsilon_2 = \langle (y^2 - x^2)/(y^2 + x^2) \rangle$ of the overlapping nuclei drives larger v_2 via partonic interactions. The nonvanishing v_3 however stems from spatial fluctuations of the participating nucleons that are inherent in AMPT [19,21]. In fact, ϵ_n ($n = 2, 3$) increases continuously with b, where $\epsilon_2 \approx \epsilon_3$ at $b \leq 3$ fm and the triangularity ϵ_3 is much smaller than ϵ_2 for peripheral collisions [21]. On the other hand, with increasing b, v_n ($n = 2, 3$) exhibits a rise and fall pattern that is much stronger in v_2 (see figure 2). Thus, the ratio v_n/ϵ_n decreases with increasing b suggesting that conversion of initial spatial asymmetry to final momentum anisotropy is less efficient for peripheral than for central collisions. The conversion efficiency is even less for higher harmonics and for smaller scattering cross-section [21].

As discussed before, the BAMPS transport with only elastic $gg \to gg$ scatterings lead to $\sim$20% smaller value of v_2. Inelastic $gg \to ggg$ scatterings is imperative [18,69,70] for a better agreement with the v_2 data. It is important to note that the extracted values of the shear viscosity-to-entropy density ratio η/s in the central region of the plasma in BAMPS [69] and AMPT [33] are rather small at $t \leq 2$ fm/c indicating that the plasma behaves almost as a perfect fluid.

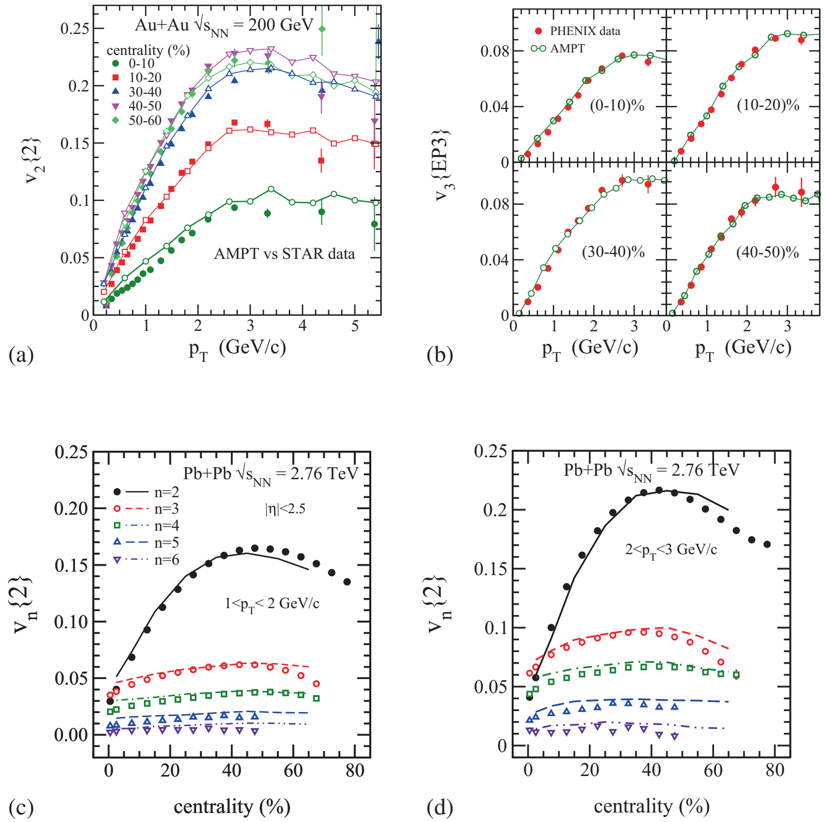

Figure 2. Top panels: p_{T} dependence of v_2 (**a**), v_3 (**b**) at various centralities at RHIC. The symbols are the STAR [65] and PHENIX [66] data. Bottom panels: Centrality dependence of v_n ($n = 2$–6) at $1 < p_{\mathrm{T}} < 2$ (**c**) and $2 < p_{\mathrm{T}} < 3$ GeV/c (**d**) at LHC. The symbols are the ATLAS data [68].

In contrast to the AMPT and BAMPS transport approaches, the Catania group [20,36,37] estimates the parton–parton scattering cross-section for various choices of η/s of the medium. Once the η/s has been fixed, the mean-field effects were found to be negligible on v_2 which is then mainly driven by the magnitude of η/s. The effect on v_2 was also studied for two cases: (i) a constant value $\eta/s = 1/4\pi$ in the hadronic and QGP phase and (ii) a constant $\eta/s = 1/4\pi$ in the QGP phase that increases as T drops below T_{c} and reaches the estimated hadronic matter value of $\eta/s \sim 8/4\pi$ [71]. At RHIC energies, $v_2(p_{\mathrm{T}})$ in the latter case is reduced by $\sim$20% compared to the constant η/s used throughout the evolution and is consistent with data. On the other hand, at LHC energies, $v_2(p_{\mathrm{T}})$ is found rather insensitive in the two scenarios. This stems from larger lifetime of the plasma at LHC which causes v_2 to fully develop in the QGP phase itself and the hadronic phase plays a minor role.

Unlike the η/s vs. T variation [71], the ratio of the electrical conductivity and temperature, σ_0/T, was shown (in PHSD [72]) to drop in hadronic matter with T, reaches a minimum at about T_{c} and remains constant above $\sim 5T_{\mathrm{c}}$. This suggests that QCD matter even at $T \approx T_c$ is a better electric conductor than Cu or Ag at room temperature. It remains to be seen how the σ_0/T variation would affect the anisotropic flow when implemented within the hydrodynamic models.

Recently, the beam energy scan (BES) programme was initiated at RHIC to map the QCD phase diagram and to locate the QCD critical point [73–75]. A larger v_2 was observed for p, K^+ and π^- relative to $\bar{p}$, K^- and π^+ at lower energies of $\sqrt{s_{NN}} = 7.7$, 11.5 and 39 GeV and v_2 becomes identical at higher $\sqrt{s_{NN}}$ [76]. This has been traced to repulsive (attractive) vector potentials for particles (antiparticles) in the hadronic phase [77]. Within a parton transport approach based on the Nambu–Jona–Lasinio (NJL) model, it was shown [78] that a relatively weak vector field is required to explain the v_2 differences between the particles (protons, lambda, kaons) and their antiparticle counterparts as observed in the BES programme at RHIC.

Recently, a new tool, namely correlations among event planes (which are higher-order correlations) corresponding to different harmonics promises to provide additional insight into the parton dynamics [79–81]. One such simplest observable is $\langle \cos(4(\Psi_{4A} - \Psi_{2B}) \rangle$, where the event-plane angle Ψ_n for harmonic n is calculated for two subevents A and B separated by pseudorapidity gap. Instead of this event-plane method, one can simply estimate the correlators by using flow vectors in harmonic n as $Q_n = |Q_n| \exp(in\Psi_n) \equiv \sum_j \exp(in\phi_j)$, where the sum runs over all particles N each with azimuth ϕ_j. Nontrivial correlations have been observed [81] and several new ones have been predicted within AMPT [22] at LHC for three- and four-plane correlators which can be tested at these facilities and would also be interesting to study in other models.

3.3 *High-p_{T} charged hadron suppression*

The phenomenon of jet quenching is another remarkable discovery at RHIC [23,24] and later at LHC [82,83] that provides tomography of the QGP formed in heavy-ion collisions. The suppression has been established as due to energy loss by the propagating hard partons in the plasma primarily by radiative gluon emission [25–31]. The suppression of high-p_{T} hadrons is quantified by the nuclear modification factor

$$R_{AA}(p_{\mathrm{T}}) = \frac{\mathrm{d}^2 N^{AA}/\mathrm{d}\eta\, \mathrm{d}p_{\mathrm{T}}}{\langle N_{\mathrm{coll}} \rangle\, \mathrm{d}^2 N^{pp}/\mathrm{d}\eta\, \mathrm{d}p_{\mathrm{T}}}, \tag{4}$$

which is the ratio of particle yield in heavy ions ($A + A$) to that in $p + p$ reference spectra, scaled by the total number of binary nucleon–nucleon collisions $\langle N_{\mathrm{coll}} \rangle$. In the absence of initial- and final-state nuclear medium effects $R_{AA}(p_{\mathrm{T}}) = 1$ by construction.

In the past decade, several jet-quenching formalisms and their numerical implementations have been developed. The BAMPS transport treats parton energy loss via explicit elastic ($gg \to gg$) and radiative ($gg \to ggg$) processes [18,34]. Within the pQCD framework, four major jet-quenching formalisms have been developed, namely, the reaction operator and path integral approaches to opacity expansion (GLV [26], BDMPS/ASW [25,29]), higher twist (HT) [27] and finite temperature field theory (AMY) [28] (for comparison of these models, see ref. [31]). All these schemes assume perturbative dynamics for jet evolution that can be factorized from the medium. Here, the modification of the hard parton depends (among other model parameters) on the p_{T} broadening imparted by the medium to the jet by collisions. The entire phenomenology of the medium is encoded in the transport coefficient $\hat{q} = \langle p_T^2 \rangle / L$ that controls the radiative energy loss. Though all the schemes within the same hydrodynamic baseline medium evolution explain the quenching data at RHIC satisfactorily, the extracted $\hat{q}$ are found largely different [31].

An alternative approach has been adopted that explicitly accounts for the jet–medium interactions [32,33,84]. It uses the approximated GLV formalism for the instantaneous jet energy loss $\Delta E \sim \alpha_s^3 \rho(\mathbf{r}(\tau), \tau) \log(2E/m_D^2 L)$, where $\mathbf{r}(\tau)$ and E are position and initial energy of the jet at time τ along its path. Within the AMPT transport as a baseline medium, ΔE can be directly obtained by estimating the local parton density $\rho(\mathbf{r}(\tau), \tau)$ and length L traversed by the jet within a time interval. Further, collision of the soft partons in the medium with both the hard jet and the gluons emitted from the lost energy can be explicitly implemented.

The nuclear modification factor R_{AA} for charged hadrons is shown in figure 3. The suppression is much smaller than in the hadronic transport HSD model [85] which clearly indicates partonic interactions. With the same parton scattering cross-section that reproduces particle yield and flow data at RHIC, the AMPT results describe the magnitude and pattern of the RHIC suppression data [23] at peripheral as well as central collisions within the GLV [26] energy loss formalism. In peripheral Pb+Pb collisions at LHC, the R_{AA} for charged hadrons is nearly constant at about 0.7 over a large p_T range. Here, the QGP even if formed, should have a small volume and short lifetime. However, in central Pb+Pb collisions at LHC, jet quenching in AMPT is distinctively overpredicted relative to ALICE and CMS measurements. This suggests that the LHC medium with a factor of 2.4 increase in density over RHIC is, in fact, more transparent [53]. This was believed to be a generic problem, as the WDGH jet energy loss model [86] that has been constrained to fit the RHIC suppression data was also found to severely underpredict the central R_{AA} at LHC.

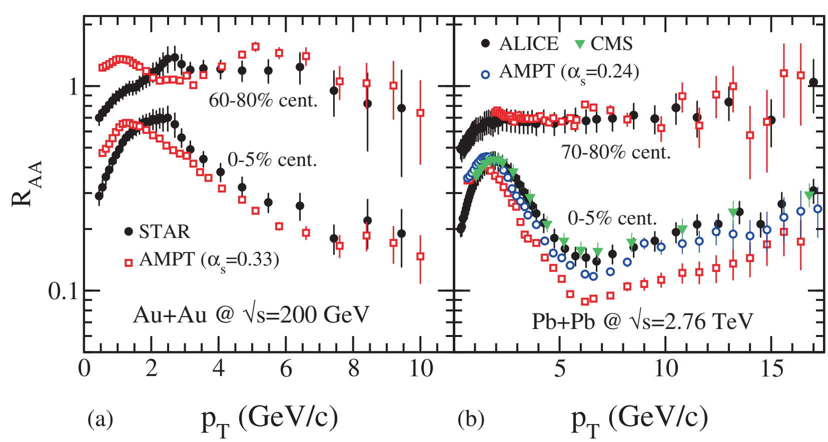

Figure 3. R_{AA} for charged hadrons as a function of p_T in central and peripheral collisions for Au+Au at RHIC (**a**) and Pb+Pb at LHC (**b**). The data are from STAR [23] at RHIC and from ALICE [82] and CMS [83] at LHC. The AMPT results are with strong coupling constant $\alpha_s = 0.33$ at RHIC and LHC and with $\alpha_s = 0.24$ for central collisions at LHC.

We however note that the scaling relation [87,88] allows one to estimate the initial temperature of the plasma to be $T_{\mathrm{i}} \approx 320$ and 436 MeV at RHIC and LHC respectively. With the adopted choice of $\alpha_{\mathrm{s}} = 0.33$ in AMPT, the parton–parton $\sigma \approx 9\pi\alpha_{\mathrm{s}}^2/(2m_{\mathrm{D}}^2) \approx 9\alpha_{\mathrm{s}}/(8T^2)$ then becomes 1.4 mb at RHIC and a much smaller value of 0.76 mb at LHC than the value of 1.5 mb used. Alternatively, if m_{D} is set constant at 3.23 fm^{-1} from RHIC to LHC, this smaller σ then gives $\alpha_{\mathrm{s}} \approx 0.24$ at LHC. With this reduced α_{s}, the AMPT results for R_{AA} (figure 3, open blue circles) in central Pb+Pb collisions at LHC is found to agree with the data. This is a clear indication of thermal suppression of the QCD coupling constant at the higher temperature reached at LHC.

As jets are typically formed in pairs and are mostly surface biased [89], the observed jet can be used as a trigger and study the remains of the balancing jet as well as particles derived from medium response by imposing energy–momentum conservation of all the particles produced in the event [32]. Within AMPT it has been found that the jet losses energy by elastic scattering with the (partonic medium) and dominantly by medium-induced gluon radiation. The remnants of the lost away-side jets appear as soft particles mostly with $p_{\mathrm{T}} < 600$ GeV/c that balances the momentum of the trigger [90].

Without any background subtraction the medium's response to the lost energy/momentum will reappear as double-peaked structure in away-side direction in the dihadron azimuthal correlation [91–93]. To purely gauge the medium's contribution to the dihadron peak, the importance of subtraction of elliptic as well as triangular flow contributions was first demonstrated within the AMPT model [19]. A careful investigation within AMPT [94] at the RHIC energy reveals that after subtraction of all v_n ($n = 1$–6) contributions, the residual dihadron in away-side peak almost disappears in central collisions but is still visible as a small peak in peripheral collisions at RHIC energy.

A Monte Carlo simulation for jet evolution with energy loss (JEWEL) [95] was developed that connects final-state parton shower with medium modification of jets with exact energy–momentum conservation at each interaction vertex. Elastic interaction was invoked via medium-induced modification of the jet as well as jet-induced modification of the medium. The collisional and radiative medium modifications exhibited characteristic differences in the jet fragmentation patterns. However, the transverse momentum of the jet shows slight increase/decrease without appreciable broadening.

4. Concluding remarks

Understanding the properties of the new state of matter — the strongly coupled quark-gluon plasma (sQGP) – formed in relativistic heavy-ion collisions at RHIC and LHC is extremely challenging. As both nonperturbative and perturbative physics play crucial roles, while QCD is not well understood in nonperturbative domain, one would take recourse to theoretical models. Transport models that explicitly invoke all the pertinent stages of collision, namely minijet and hard parton production in nucleon–nucleon collisions, parton transport, hadronization and finally hadron transport, is ideally suited to study and predict the properties of the sQGP. Several transport models with varying underlying physics content encoding the medium have been developed. These models have been quite successful in explaining a large body of data at these energies.

Independent transport model analysis of bulk matter observables, such as hadron yield distributions, anisotropic flow, clearly underscores the importance of either a large initial parton density (AMPT model [17]) or three-body gluonic interactions (BAMPS model [34]), or scalar and vector mean field for the partons (PHSD model [35]) or parton–parton scattering cross-section derived from $\eta/s(T)$ that behaves as predicted in lattice QCD (model of Catania group [20]). The most ideal transport model should incorporate all these features simultaneously which can then be used to study their relative importance during the evolution of the medium at various beam energies.

Complementary to the bulk observables, another important challenge at present is to understand the jet quenching mechanism and how the medium's response to the lost energy and momentum will eventually be manifested and whether this mechanism can be used to explore the plasma properties. To date most theoretical studies about jet energy loss and jet observables have been based on simple fireball model or hydrodynamic model for the underlying medium propagation, whereas, microscopic transport models allow a realistic approach to jet-quenching studies via explicit incorporation of both the jet–medium interaction and the medium's response to the jet and emitted gluons. However, to date there is no general and well-established theory for the interaction of hard jets with the medium which represents a major impediment in the use of jet quenching to extract the QGP properties. Further, there are many important conceptual issues such as implementation of multigluon emission, their transverse momentum broadening, jet-induced medium modifications and hadronization of the emitted/scattered gluons in the medium. Once these issues are resolved and the jet-quenching description is available from first principles, one can incorporate the complex jet physics within the transport models which in turn can be used as comprehensive probe of the deconfined matter properties. In conjunction with the bulk and jet observables, the transport models, with all the features consistently incorporated, can potentially predict new physics and exciting properties of the quark-gluon plasma formed at the RHIC and the LHC energies.

References

[1] I Arsene *et al*, *Nucl. Phys. A* **757**, 1 (2005)
[2] B B Back *et al*, *Nucl. Phys. A* **757**, 28 (2005)
[3] J Adams *et al*, *Nucl. Phys. A* **757**, 102 (2005)
[4] K Adcox *et al*, *Nucl. Phys. A* **757**, 184 (2005)
[5] ALICE Collaboration: J Schukraft, *J. Phys. G* **38**, 124003 (2011)
[6] ATLAS Collaboration: P Steinberg, *J. Phys. G* **38**, 124004 (2011)
[7] CMS Collaboration: B Wyslouch, *J. Phys. G* **38**, 124005 (2011)
[8] M Gyulassy and L McLerran, *Nucl. Phys. A* **750**, 30 (2005)
[9] E V Shuryak, *Nucl. Phys. A* **750**, 64 (2005)
[10] P Romatschke and U Romatschke, *Phys. Rev. Lett.* **99**, 172301 (2007)
P Romatschke, *Int. J. Mod. Phys. E* **19**, 1 (2010)
[11] H Song and U W Heinz, *Phys. Lett. B* **658**, 279 (2008); *Phys. Rev. C* 81 024905 (2010)
[12] G S Denicol, T Koide and D H Rischke, *Phys. Rev. Lett.* **105**, 162501 (2010)
[13] A Jaiswal, R S Bhalerao and S Pal, *Phys. Lett. B* **720**, 347 (2013)
[14] S Pratt, *Phys. Rev. Lett.* **102**, 232301 (2009)
[15] Z W Lin, C M Ko and S Pal, *Phys. Rev. Lett.* **89**, 152301 (2002)
[16] R S Bhalerao, J-P Blaizot, N Borghini and J-Y Ollitrault, *Phys. Lett. B* **627**, 49 (2005)
[17] Z W Lin, C M Ko, B-A Li, B Zhang and S Pal, *Phys. Rev. C* **72**, 064901 (2005)
[18] O Fochler, Z Xu and C Greiner, *Phys. Rev. Lett.* **102**, 202301 (2009)

[19] B Alver and G Roland, *Phys. Rev. C* **81**, 054905 (2010), Erratum, *ibid. C* **82**, 039903 (2010)
[20] G Ferini, M Colonna, M Di Toro and V Greco, *Phys. Lett. B* **670**, 325 (2009)
[21] L X Han *et al*, *Phys. Rev. C* **84**, 064907 (2011)
[22] R S Bhalerao, J-Y Ollitrault and S Pal, *Phys. Rev. C* **88**, 024909 (2013)
[23] J Adams *et al*, *Phys. Rev. Lett.* **91**, 172302 (2003)
[24] S S Adler *et al*, *Phys. Rev. C* **69**, 034910 (2004)
[25] R Baier, Y L Dokshitzer, A H Mueller, S Peigne and D Schiff, *Nucl. Phys. B* **483**, 291 (1997)
[26] M Gyulassy, P Levai and I Vitev, *Phys. Rev. Lett.* **85**, 5535 (2000)
[27] X F Guo and X N Wang, *Phys. Rev. Lett.* **85**, 3591 (2000)
[28] P Arnold, G D Moore and L G Yaffe, *J. High Energy Phys.* **0206**, 030 (2002)
[29] N Armesto, C A Salgado and U A Wiedemann, *Phys. Rev. D* **69**, 114003 (2004)
[30] M Gyulassy, I Vitev, X N Wang and B W Zhang, in *Quark gluon plasma* edited by R C Hwa and X N Wang (World Scientific, Singapore, 2004)
A Kovner and U A Wiedemann, in: *Quark gluon plasma* edited by R C Hwa and X N Wang (World Scientific, Singapore, 2004)
[31] S A Bass, C Gale, A Majumder, C Nonanka, G-Y Qin, T Renk and J Ruppert, *Phys. Rev. C* **79**, 024901 (2009)
[32] S Pal and S Pratt, *Phys. Lett. B* **574**, 21 (2003)
[33] S Pal, *Phys. Rev. C* **80**, 041901(R) (2009)
[34] Z Xu and C Greiner, *Phys. Rev. C* **71**, 064901 (2005); *ibid.* **76**, 024911 (2007)
[35] E L Bratkovskaya, W Cassing, V P Konchakovski and O Linnyk, *Nucl. Phys. A* **856**, 162 (2011)
[36] V Greco, M Colonna, M Di Toro and G Ferini, *Prog. Part. Nucl. Phys.* **62**, 562 (2009)
[37] M Ruggieri, F Scardina, S Plumari and V Greco, arXiv:1312.6060 [nucl-th]
[38] X N Wang and M Gyulassy, *Phys. Rev. D* **44**, 3501 (1991)
[39] W-T Deng, X-N Wang and R Xu, *Phys. Rev. C* **83**, 014915 (2011); *Phys. Lett. B* **701**, 133 (2011)
[40] D W Duke and J F Owens, *Phys. Rev. D* **30**, 49 (1984)
[41] M Glück, E Reya and W Vogt, *Z. Phys. C* **67**, 433 (1995)
[42] W Cassing and E L Bratkovskaya, *Phys. Rep.* **308**, 65 (1999)
[43] A Peshier, *Phys. Rev. D* **70**, 034016 (2004)
[44] W Cassing, *Nucl. Phys. A* **791** (2007); *ibid.* **795**, 70 (2007)
[45] F Karsch, E Laermann and A Peikert, *Nucl. Phys. B* **605**, 579 (2001)
[46] A Bazavov *et al*, *Phys. Rev. D* **80**, 014504 (2009)
[47] B Zhang, *Comput. Phys. Commun.* **109**, 193 (1998)
[48] B Zhang, L W Chen and C M Ko, *J. Phys. G* **35**, 065103 (2008)
[49] Y Aoki *et al*, *J. High Energy Phys.* **0906**, 088 (2009)
[50] B-A Li and C M Ko, *Phys. Rev. C* **52**, 2037 (1995)
[51] H Sorge, *Phys. Rev. C* **52**, 3291 (1995)
[52] S Scherer *et al*, *Prog. Part. Nucl. Phys.* **42**, 279 (1999)
[53] S Pal and M Bleicher, *Phys. Lett. B* **709**, 82 (2012)
[54] I G Bearden *et al*, *Phys. Rev. Lett.* **88**, 202301 (2002)
[55] S S Adler *et al*, *Phys. Rev. C* **71**, 034908 (2005)
[56] K Aamodt *et al*, *Phys. Rev. Lett.* **106**, 032301 (2011)
[57] J Xu and C M Ko, *Phys. Rev. C* **83**, 034904 (2011)
[58] J-Y Ollitrault, *Phys. Rev. D* **46**, 229 (1992)
[59] S A Voloshin, A M Poskanzer and R Snellings, arXiv:0809.2949 [nucl-ex]
[60] N Borghini, P M Dinh and J-Y Ollitrault, *Phys. Rev. C* **64**, 054901 (2001)
[61] M Bleicher and H Stoecker, *Phys. Lett. B* **526**, 309 (2002)
[62] E L Bratkovskaya, W Cassing and H Stöcker, *Phys. Rev. C* **67**, 054905 (2003)

[63] D Molnar and M Gyulassy, *Nucl. Phys. A* **697**, 495 (2002), Erratum, *ibid. A* **703**, 893 (2002)
[64] D Molnar and P Huovinen, *Phys. Rev. Lett.* **94**, 012302 (2005)
[65] S S Adler *et al*, *Phys. Rev. C* **72**, 014904 (2005)
[66] A Adare *et al*, *Phys. Rev. Lett.* **107**, 252301 (2010)
[67] K Aamodt *et al*, *Phys. Rev. Lett.* **105**, 252302 (2010)
[68] G Aad *et al*, *Phys. Rev. C* **86**, 014907 (2012)
[69] Z Xu, C Greiner and H Stocker, *Phys. Rev. Lett.* **101**, 082302 (2008)
[70] Z Xu and C Greiner, *Phys. Rev. C* **79**, 014904 (2009)
[71] L P Csernai, J I Kapusta and L D McLerran, *Phys. Rev. Lett.* **97**, 152303 (2006)
[72] W Cassing, O Linnyk, T Steinert and V Ozvenchuk, *Phys. Rev. Lett.* **110**, 182301 (2013)
[73] Z Fodor and S D Katz, *J. High Energy Phys.* **0203**, 014 (2002)
[74] S Ejiri, C R Allton, S J Hands, O Kaczmarek, F Karsch, E Laermann and C Schmidt, *Prog. Theor. Phys. Suppl.* **153**, 118 (2004)
[75] R V Gavai and S Gupta, *Phys. Rev. D* **71**, 114014 (2005)
[76] STAR Collaboration: B Mohanty, *J. Phys. G* **38**, 124023 (2011)
[77] J Xu, L-W Chen, C M Ko and Z-W Lin, *Phys. Rev. C* **85**, 041901 (2012)
[78] T Song, S Plumari, V Greco, C M Ko and F Li, arXiv:1211.5511 [nucl-th]
[79] R S Bhalerao, M Luzum and J-Y Ollitrault, *Phys. Rev. C* **84**, 034910 (2011)
[80] K Aamodt *et al*, *Phys. Rev. Lett.* **107**, 032301 (2011)
[81] ATLAS Collaboration: J Jia, *Nucl. Phys. A* **910–911**, 276 (2013)
[82] K Aamodt *et al*, *Phys. Lett. B* **696**, 30 (2011)
[83] S Chatrchyan *et al*, *Eur. Phys. J. C* **72**, 1945 (2012)
[84] T Hirano and Y Nara, *Phys. Rev. C* **66**, 041901 (2002)
[85] K Gallmeister and W Cassing, *Nucl. Phys. A* **748**, 241 (2005)
[86] W A Horowitz and M Gyulassy, *Nucl. Phys. A* **872**, 265 (2011)
[87] M Gyulassy and T Matsui, *Phys. Rev. D* **29**, 419 (1984)
[88] S Pal and S Pratt, *Phys. Lett. B* **578**, 310 (2004)
[89] H Zhang, J F Owens, E Wang and X-N Wang, *Phys. Rev. Lett.* **98**, 212301 (2007)
[90] S Chatrchyan *et al*, *Phys. Rev. C* **84**, 024906 (2011)
[91] J Adams *et al*, *Phys. Rev. Lett.* **95**, 152301 (2005)
[92] A Adare *et al*, *Phys. Rev. C* **78**, 014901 (2008)
[93] B I Abelev *et al*, *Phys. Rev. Lett.* **102**, 052302 (2009)
[94] J Xu and C M Ko, *Phys. Rev. C* **84**, 014903 (2011); *ibid.* **84**, 044907 (2011)
[95] K Zapp, G Ingelman, J Rathsman, J Stachel and U A Wiedemann, *Eur. Phys. J. C* **60**, 617 (2009); *Indian J. Phys.* **85**, 1033 (2011)